Scientific Research Publishing

Journal of Transportation Technologies, 2025, 15(1), 122-134
https://www.scirp.org/journal/jtts
ISSN Online: 2160-0481
ISSN Print: 2160-0473

Simulation of Auxiliary Magnetorheological Brake on Vehicles

Quang Tuan Hoang[1,2], Minh Hoang Trinh[1], Thanh-Tung Nguyen[1]

[1]School of Mechanical Engineering, Hanoi University of Science and Technology, Hanoi, Vietnam
[2]School of Mechanical and Automotive Engineering, Hanoi University of Industry, Hanoi, Vietnam
Email: tung.nguyenthanh@hust.edu.vn

How to cite this paper: Hoang, Q.T., Trinh, M.H. and Nguyen, T.-T. (2025) Simulation of Auxiliary Magnetorheological Brake on Vehicles. *Journal of Transportation Technologies*, **15**, 122-134.
https://doi.org/10.4236/jtts.2025.151007

Received: October 24, 2024
Accepted: January 14, 2025
Published: January 17, 2025

Abstract

In ground vehicles, the brake is an essential system to ensure the safety of movement. Multiple braking mechanisms have been introduced for use in vehicles. This study explores the potential of using magneto-rheological fluid (MRF) brakes in automotive applications. MRF brakes offer controllable braking force due to a magnetic field, but their use is limited by simulation challenges. In this study, a 7-tooth MRF brake model is proposed. The brake model is simulated in Altair Flux software to analyze magnetic field distribution, braking torque, and its variation under different currents and disc speeds. The simulation conditions also consider both viscous and electromagnetic torque components. Then, the results are analyzed across different brake regions, including rotor, stator, and fluid gap. These results provide valuable insights for designing, manufacturing, installing, and testing MRF brakes for automotive use.

Keywords

Magnetorheological Fluid (MRF), Magnetorheological Brake (MRB), Simulation, Automotive Applications, Altair Flux Software

1. Introduction

Braking systems play a critical role in ensuring the safety of automobiles, especially with the continuous advancements in technology and the increasing speeds of vehicles. The need for innovation and adoption of new technologies in braking systems is becoming increasingly essential. Various auxiliary braking systems have been researched and implemented to enhance safety, comfort, and ease of control. In recent years, technological advancements, particularly in microprocessors, sensors, electronic devices, and processing speeds, have opened the possibility of real-time

control for intelligent systems utilizing magnetorheological (MR) fluids. A potential application of this technology is the MR brake system in automobiles. Current research on MR brakes for automobiles focuses on key issues such as:

- Magnetic Circuit Analysis and Design, Optimization of MR Brake Design for Improved Braking Performance;
- MR Brake Thermal Analysis for Ensuring Stable and Safe Operation under High-Temperature Conditions;
- Research on Methods to Reduce No-Load Torque of MR Brakes for Improved Energy Efficiency when the System is Deactivate;
- MRB Brake Control Strategy for Efficient Integration with the Main Brake System and Ensuring Flexible Operation [1]-[3].

Analysis and design of MR brakes is a crucial research area for the development of efficient and energy-saving braking systems. Extensive research has been conducted to optimize MR brake performance and reduce brake mass [4]-[9]. MR brake optimization studies employ optimization techniques to identify the optimal values of MR brake design parameters [10]-[12]. The goal is to achieve the highest braking performance. A limitation of conventional MRB designs is the generation of viscous torque due to the interaction between the MR fluid and its interacting surfaces. This viscous torque causes energy loss and can negatively affect the lifespan of the MR fluid. Numerous studies have focused on mitigating this interaction and proposed measures to reduce viscous torque generation [12]-[16].

Another important design consideration in MRB research is the long-term effect of temperature (due to heat buildup) on the degradation of MR fluid properties. Thermal studies of MRBs have been conducted independently for both general MR brake devices and specifically for MRBs mounted on vehicles. Some thermal studies are often performed using numerical simulation methods, followed by experimental verification to determine the temperature distribution on MR brake components such as the rotor, stator, and MR fluid layer [6] [17]-[20].

The objective of this study is to simulate an MRB that works under a similar working condition to that of a specific vehicle. The position of the MRB is shown in **Figure 1**. Section 2 introduces the MRB structure with coil configuration and simulation setup. In Section 3, the results are analyzed considering braking torque, supply current, and oil resistance. The results show that the proposed MRB has performed well under the predefined conditions and can be used as a reference for future development.

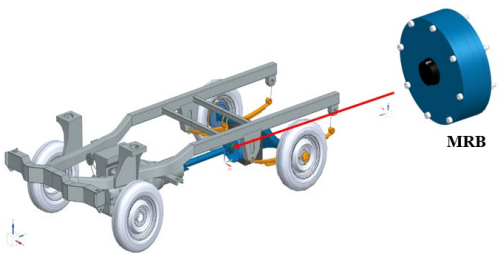

Figure 1. Layout of the magnetic brake on a small truck.

2. Methodology

2.1. MRB Design

This study used a proposed design of MRB by Nguyen A.N. [21]: a disc-type MRB brake structure with 7 trapezoidal teeth, which are 75 degrees inclined grooves on the disc surface, and the MR fluid gap is 1 mm. The MRB is supplied with a current from 0 - 3 A for the 2 coils placed on the two halves of the brake housing. Each coil has 1000 turns, and the wire diameter is 0.5 mm. A small gap of 1 mm filled with magnetic fluid is maintained between the disc and the housing.

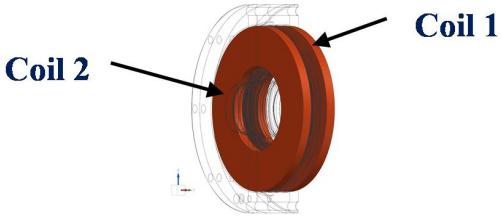

Figure 2. Model of MRB and coils placement.

At the time of braking, the electromagnet integrated into the housing is energized. Due to the magnetorheological effect, the MR fluid inside the magnetic field becomes semi-solid as the viscosity increases within a few milliseconds, and shear friction occurs along the disc surface, resulting in braking and hence deceleration. However, this effect is reversible, meaning that the viscosity of the MRF decreases, and it returns to a liquid state. The MRB operates in shear mode. In this study, a disc brake with trapezoidal teeth grooves on the surface is used. **Figure 2** shows the main structure of the MRB with rotor, braking housing and coils:

- The rotor is mounted on the Cardan shaft, the active shaft housing, the trapezoidal disc shape, and the trapezoidal angle is 75 degrees.
- The brake housing is assembled from steel plates with circular holes for bolting and holes for the coils.

2.2. Magnetic Field Simulation Using Altair-Flux Software

The MRB CAD model was first constructed, and then a finite element model was processed with the HYPERMESH tool (**Figure 3**). The stability was checked using the Altair Engineering Flux solver. The material used in the MRB model was C45 steel and MRF-140CG oil [22]. Two copper coils were placed in the MRB cavity and the current flowing through the copper wire was controlled to a predetermined value. The current boundary condition is determined by the current value flowing through the brake coil. For the magnetic field analysis problem, the current value considered is from 0 A to 3 A, with a gradual increase of 0.25 A. To increase the magnetic field intensity, the two coils on both sides will be supplied with current in the opposite direction. The finite element model is constructed with a mesh size of 4 mm, with 337050 nodes and 1496943 elements. The tetrahedron elements method was used to create the meshing model. For this meshing

model, it's crucial to carefully consider the mesh size to ensure accurate magnetic field interactions between different surfaces. The optimal size will depend on the desired level of detail. In this case, an average mesh size of 0.5 was chosen. The details of meshing parameters are shown in Table 1.

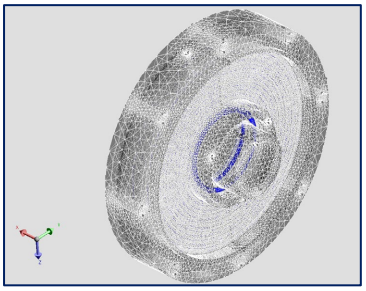

Figure 3. Meshing the model Meshing the model Meshing the model.

Table 1. Meshing parameters.

Number of elements	
Number of nodes	487157
Number of line element	48996
Number of surface element	433402
Number of volume element	2909637
Element quality	
Number of parts not evaluated	0%
Part numbers of good quality	98.59%
Average number of quality elements	1.1%
Number of low-quality parts	0.01%

2.3. Calculation Method of the Brake Torque Generated in the Simulation

The braking torque is calculated based on the Bingham rheological model of MRF. To calculate the torque for this structure, the study refers to the method of calculating the braking torque of a similar "passive" disc brake structure [23].

To simplify the analysis and calculation of the forces and torques generated by MRF, the following assumptions are applied:

- The fluid is incompressible and flows steadily in layers;
- The effects of gravity and centrifugal force of the MRF element are neglected;
- The radial and axial velocities are zero;
- The fluid is assumed to be in full contact with the disc and does not slip;
- Due to the very small gap size being investigated, the fluid flow is fully plastic, with no solid region and neglecting axial motion.

The braking torque is calculated based on the magnetic field intensity of the simulation and the dimensions of the magnetic brake model. Figure 4 shows the details of regions that contributed to the braking torque. The equation for calculating the torque is given in the theoretical calculation section based on the Bingham model when neglecting bearing friction as follows:

$$T_{\Sigma} = 2\left(T_e + T_a\right) + T_c \tag{1}$$

where:

T_e—Total braking torque in the oil layer perpendicular to the rotor axis;

T_a—Total braking torque in the oil layer at an angle;

T_c—Braking torque of the outermost oil layer.

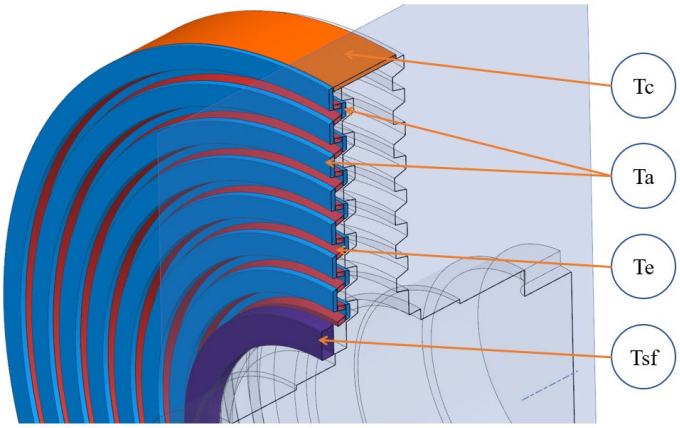

Figure 4. Torque generating oil regions of MRB Brake.

The torque generated from Region A (tilted regions) is determined based on the Bingham fluid model. A small ring element in the tilted MRF gap is considered, as shown in **Figure 5**. The friction torque acting on this element can be formulated as:

$$dT = r\tau dA = 2\pi r2\tau dl = 2\pi\left(R1 + l\sin\varphi\right)2\tau dl \tag{2}$$

where:

r—the calculation radius of the considered fluid element in the tilted oil-filled herringbone groove (m), $R1$, $R2$ are the calculation radius at the tooth root and tip according to the trapezoidal cross-section (m).

l—the length of the inclined tooth section, l = La/cosφ

La is the length of the oil film calculated on the rotation axis from $R1$ to $R2$ (m)

Φ is the angle of inclination of the trapezoidal surface (rad). The cutting speed of MRF in the tube is approximated as: $\dot{\gamma} = r\Omega/d$.

Ω—the rotational speed of the rotating disk (rad/s), d is the gap of the oil MRF (m).

Bingham Model of MRF along the Axial direction

$$\tau = \tau_y + \mu\frac{r\Omega}{d} = \tau_y + \mu\frac{\Omega\left(R_1 + 1\sin\varphi\right)}{d} \tag{3}$$

Thus, the torque generated from Region A can be formulated as:

$$\begin{aligned} T_a = \sum T_{ai} = {} & 2\pi\left(R_{2i-1}^2 l + R_{2i-1} l^2 \sin\varphi + \frac{1}{3} l^3 \sin^2\varphi\right)\tau_{ya2i-1} \\ & + \frac{1}{2}\pi\mu_{a2i-1}\frac{\Omega}{d}\left(4lR_{2i-1}^3 + 6R_{2i-1}^2 l^2 \sin\varphi + 4R_{2i-1} l^3 \sin^2\varphi + l^4 \sin^3\varphi\right)(i = 1\text{ - }15) \end{aligned} \tag{4}$$

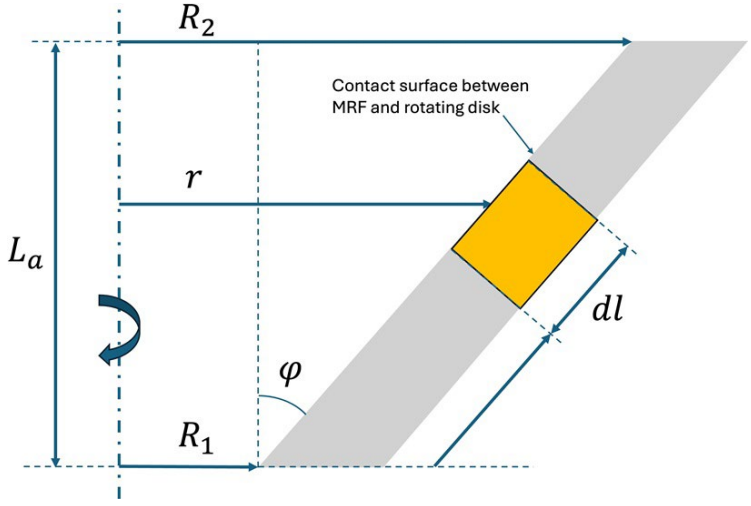

Figure 5. Calculation model of braking torque generated by MRB in Region A.

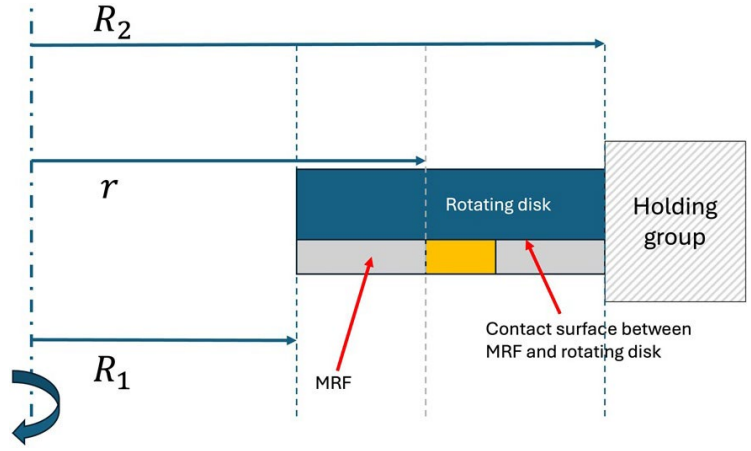

Figure 6. Calculation model of braking torque generated by MRB in Region E.

Torque generated from Region E (**Figure 6**):

$$T_e = \sum T_{ej} = \frac{\pi \mu_{ej} R_j^4}{2d}\left[1 - \left(\frac{R_j}{R_{j+1}}\right)^4\right]\Omega + \frac{2\pi\tau_{yej}}{3}\left(R_{j+1}^3 - R_j^3\right)\left(j = 1 \text{ - } 16\right) \quad (5)$$

Torque generated from the Oil Region and Bearing:

$$T_{sf} = 0.65\left(2R_s\right)^2 \Omega^{\frac{1}{3}} \quad (6)$$

where:

T_{sf}—the torque generated at the oil-bearing region (Nm)

R_s—the shaft radius at the bearing mounting location (m).

Torque generated from Region C:

$$T_c = 2\pi R_d^2 b\left(\tau_{yc1} + \mu_{c1}\frac{\Omega R_d}{d}\right) \quad (7)$$

where:

T_c—the torque at Region C (Nm);

R_d—the outer radius of the rotor disk (m);

b—the tooth thickness at the outermost position (m).

τ_{yc1} —the yield stress of the oil film at Region C (N/m^2). The stress generated by the current has an intensity that depends on the characteristics of each type of oil used, the intensity generated in different areas of the brake disc as well as the geometric parameters of the MRB brake such as the radius of the oil positions surveyed relative to the center of rotation Ri, oil gap d, angular velocity of the brake disc shaft Ω, tooth thickness b.

The oil code used in the study is MRF-140CG Magneto-Rheological Fluid [22]. According to the specification, the stress-magnetic field intensity characteristic curve was constructed as shown in **Figure 7**. By applying the least squares method to fit the properties of the fluid, the approximate polynomial of the yield stress as a function of the magnetic field is determined [24]:

$$\tau_y = f\left(H_{MR}\right) = k_0 + k_1 H_{MR}^1 + k_2 H_{MR}^2 + k_3 H_{MR}^3 + k_4 H_{MR}^4 + k_5 H_{MR}^5 \quad (8)$$

In which HMR is the magnetic field intensity generated by MRF - 140CG, with the coefficients: $k_0 = 1.9$; $k_1 = 0.61$; $k_2 = -0.002$; $k_3 = 2.69 * 10^{-6;}$ $k_4 = -7.52 * 10^{-9}$; $k_5 = 1.76 * 10^{-11}$. The generated magnetic field intensity H will be applied to Equation (8) to calculate the shear stress for MR fluid, from which the torque generated by MRF can be calculated.

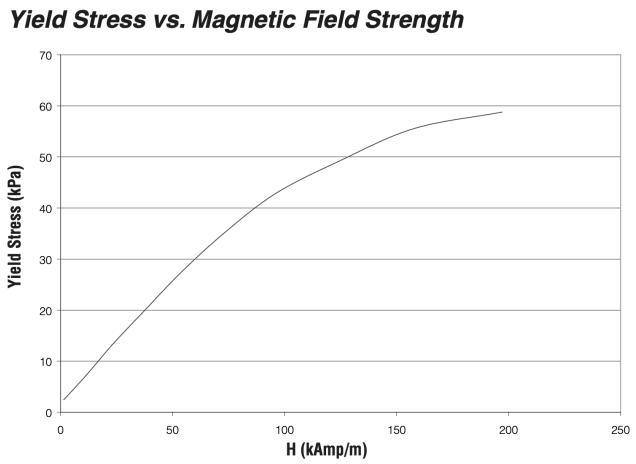

Figure 7. Characteristics of 140-CG oil. [22]

3. Results and Discussion

3.1. Magnetic Field Intensity

MR brake model is simulated at varying current values from 0 A to 3 A, and it was observed that the maximum magnetic field intensity appearing in the MR brake regions also increased to 63.5 kA/m, as shown in **Figure 8**. However, the variation pattern of the magnetic field intensity generated in the MR brake regions, as well as the path of the magnetic flux lines in the investigated cases are quite similar.

Figure 9 illustrates the generated magnetic flux density, and flux lines of the MR oil brake model when the current intensity supplied to the brake is 3 A. In this model, there are two coils arranged symmetrically around the brake disc. When the current is applied to the coils, it creates a magnetic field in the space between the coils. This magnetic field exerts a force on the iron particles in the MR fluid, causing them to move and create the MRB braking torque.

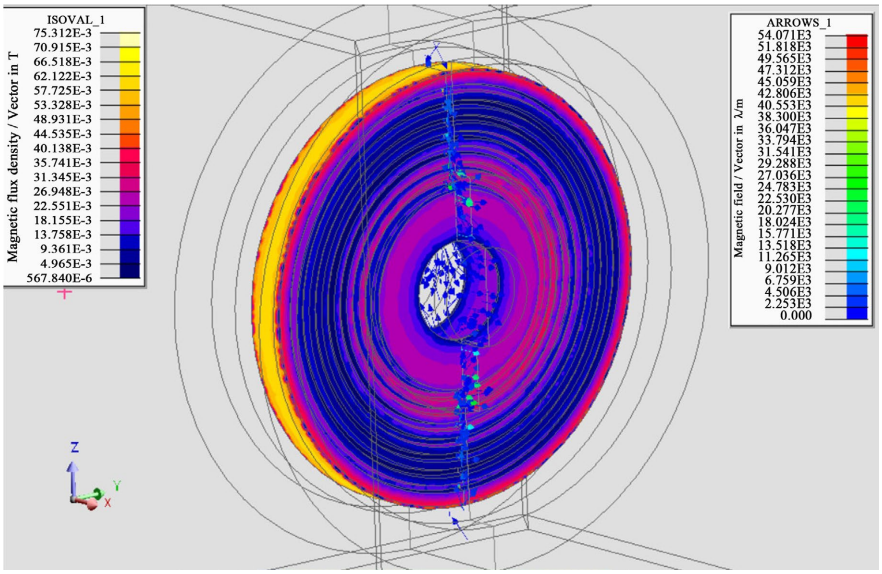

Figure 8. Magnetic field intensity generated when current intensity I = 3 A.

Moreover, it can be observed that the magnetic field intensity is the highest in the region between the coils. Due to the symmetrical arrangement of the coils, the magnetic field between coils is uniform. The magnetic field intensity in the region surrounding the coils decreases gradually as it moves away from the coils. This is because the magnetic field generated by the coils decreases gradually with distance. The region outside the brake has a very low magnetic field intensity in this region. This is because the magnetic field generated by the coils cannot penetrate the brake components.

The simulation results show that the non-uniform distribution of the magnetic flux lines on the brake disc is one of the factors leading to the difference in braking torque generated in different areas of the brake. This is because the longitudinal and inclined teeth are located in the area between the two coils, which are most affected by the magnetic field intensity. Therefore, the torque generated in these two areas accounts for a large proportion. While the horizontal teeth have a working length much smaller than the longitudinal and inclined teeth, they are affected perpendicularly by the magnetic flux lines generated by the two coils. Therefore, the braking torque generated at the horizontal teeth is also the smallest. However, there is only one horizontal tooth, so the ratio of the torque generated by the horizontal tooth to the total torque of the longitudinal and inclined teeth is quite large.

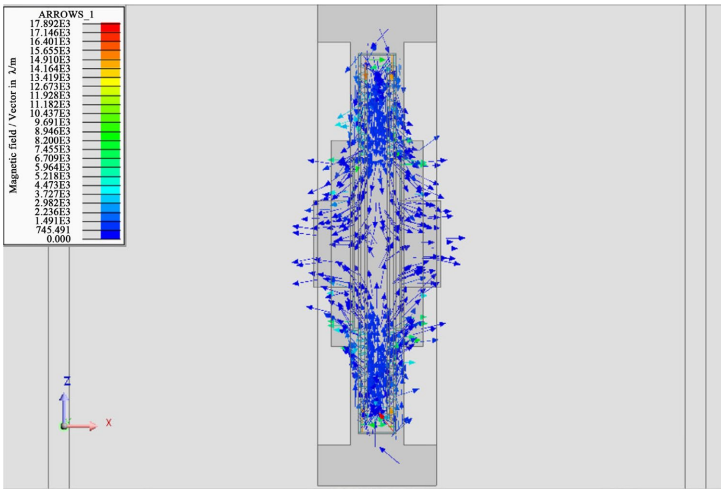

Figure 9. Magnetic flux density, and flux lines of MRB.

3.2. MRB Braking Torque when Changing the Rotor Rotation Speed

Simulation results of MRB braking torque depending on the revolutions of the brake disc shaft are shown in **Figure 10**. The maximum value of the braking torque generated by the MRB is 108 Nm, achieved at a current of 3 A and the rotor speed of 2500 RPM. The minimum value of the braking torque is 0 Nm, at no current is applied (I = 0 A), and the rotor speed is 0 RPM, and this non-magnetic field viscous torque value will increase with increasing brake disc speed. When the MRB rotor speed increases, the braking torque also increases, but with increasing revolutions, the braking torque increases more slowly. When the MRB rotor speed = 0 RPM, the magnetic oil particles are stationary. Therefore, the electromagnetic force generated by the electromagnetic coils acting on the magnetic oil particles will create the smallest braking torque with the same current intensity investigated. When the MRB rotor speed is 2500 RPM, the magnetic oil particles move at a high speed. Therefore, the shear stress caused by MR oil increases, resulting in increased braking torque with the same current intensity investigated.

The results of the viscosity of the MR oil when applying current (T_H), and the torque generated on different regions of the MR brake disc (T_a, T_e, T_c), depending on the number of brake disc revolutions are shown in **Figure 11(a)** and **Figure 11(b)**.

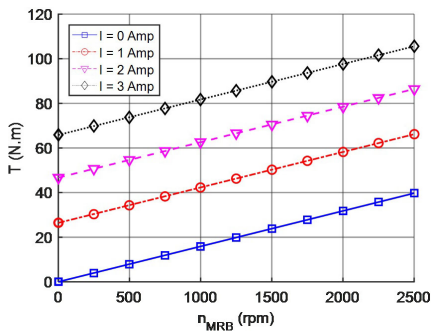

Figure 10. Relationship between MRB braking torque and rotor shaft speed.

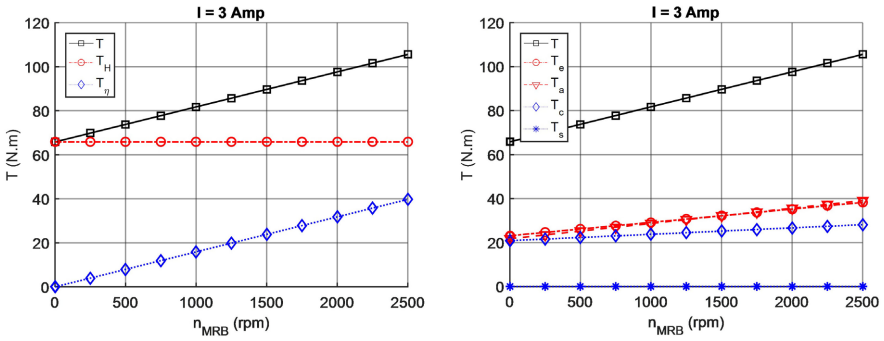

(a) (b)

Figure 11. Investigation results of braking torque—number of revolutions by oil region and drag source on MRB.

Figure 11(a) shows the braking torque generated by two viscous components of the oil, including the dynamic viscosity component (T_η) and the magnetic field viscosity component (T_H). At a current of 3 A, as the brake disc speed increases, the magnetic field torque component (T_H) remains constant, while the dynamic viscosity torque component (T_η) increases linearly from 0 to about 40 Nm. This demonstrates the clear influence of speed on the braking torque of MRB when the current is fixed. **Figure 12** shows the braking torque and rotation speed when changing the supply current.

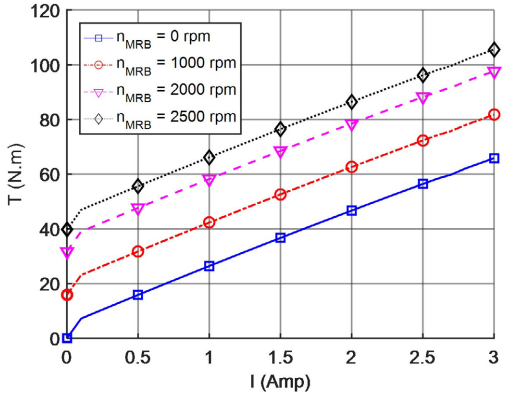

Figure 12. Braking torque—current intensity characteristic graph in simulation with speed changing from 0 - 2500 RPM.

3.3. MRB Braking Torque When Changing the Excitation Current

The braking torque generated by the MRB increases almost linearly with the current intensity. As the current intensity increases, the braking torque also increases. When the MRB rotor speed increases, the braking torque also increases quite evenly. When the MRB rotor speed is 0 RPM, the magnetic field particles are stationary. Therefore, the electromagnetic force generated by the electromagnetic coils acting on the magnetic field particles will only create a braking torque due to the magnetic field of the coils. Therefore, the braking torque in this state is 0 Nm. At a rotor speed of 2500 RPM, the magnetic field particles move at a higher speed. The electromagnetic force

generated by the electromagnetic coils acting on the magnetic field particles will be reduced, and therefore, the braking torque will also decrease.

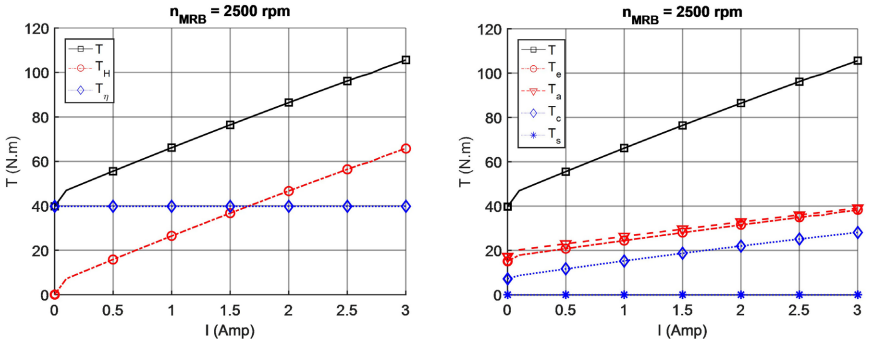

(a) (b)

Figure 13. Investigation results of braking torque when changing current intensity according to oil region and drag source on MRB.

In addition, other factors that affect the braking torque are also considered: the viscous drag torque of the MR oil and the drag torque generated by the magnetic field when the current intensity changes. **Figure 13(a)** shows the torque generated by the two components of the oil viscosity, including the conventional viscosity component (T_η) and the magnetic field viscosity component (T_H). At the investigated speed of 2500 RPM, when the current intensity increases, the torque T_η remains almost constant, reaching a value of about 40 Nm. Conversely, the T_H torque increases quite linearly from 0 to about 65 Nm. At a current intensity of 1.5 A and above, the increase in T_τ is more obvious than T_η. This is due to the working characteristics of MR oil, in which the magnetic field viscosity component (T_H) accounts for a larger proportion than the conventional viscosity component (T_η) when the current intensity increases. **Figure 13(b)** shows the braking torque generated in the longitudinal tooth (T_e), inclined tooth (T_a) and horizontal tooth (T_c) regions of the brake disc. The simulation results show that the braking torque of T_e, T_a and T_c all increase as the current intensity increases, with a uniform increase rule. The values of T_e and T_a braking torque are not much different, while T_c has the smallest value. This result is consistent with the simulation results of magnetic field intensity H, magnetic flux density B, and magnetic flux lines shown above.

The results show that the MR braking torque is directly proportional to the current intensity applied to the MRB brake. When the current reaches around 1.5 A, the magnetic force acting on the iron particles in the MR oil is large enough to overcome the dynamic drag of the MR oil, making the magnetic braking torque greater than the dynamic drag torque. This phenomenon is consistent with previous studies on MR fluid models.

4. Conclusion

The paper presents the simulation results of the braking torque characteristics of

a 7-tooth trapezoidal brake disc mechanism. The simulation results of the magnetic field in the brake disc regions show that the magnetic field is unevenly distributed in the air gap, concentrated in the area near the tooth edges of the stator and rotor. The braking torque generated by the MRB increases with the current intensity and the speed of the brake disc and can reach 108 Nm when the current intensity is 3 A and the speed of the brake disc is 2500 rpm. Thus, the MRB brake has the potential to be applied to automobiles as an auxiliary brake system. The research results can be used as a basis for the design, manufacturing and installation of directional MRBs for auxiliary brake systems on automobiles.

Acknowledgements

This research was supported and funded by Hanoi University of Science and Technology (HUST) under project number T2022-PC-035.

Conflicts of Interest

The authors declare no conflicts of interest regarding the publication of this paper.

References

[1] Zainordin, A.Z., Mohamed, Z. and Ahmad, F. (2021) The Magnetorheological Fluid: Testing on Automotive Braking System. *International Journal of Automotive and Mechanical Engineering*, **18**, 8577-8584. https://doi.org/10.15282/ijame.18.1.2021.16.0651

[2] Wang, D., Yang, G., Luo, Y., Fang, S. and Dong, T. (2023) Optimal Design and Stability Control of an Automotive Magnetorheological Brake Considering the Temperature Effect. *Smart Materials and Structures*, **32**, Article ID: 025020. https://doi.org/10.1088/1361-665x/acb1e2

[3] Kamble, R. and Patil, S. (2019) Exploring Magnetorheological Brake Based Anti-Lock Brake System for Automotive Application: Exploring MRB-Based ABS for Automotive Application. https://orcid.org/0000-0003-2653-9605

[4] Bydon, S. (2002) Construction and Operation of Magnetorheological Rotary Brake. *Archiwum Process Control*, 20.

[5] Liu, B., Li, W.H., Kosasih, P.B. and Zhang, X.Z. (2006) Development of an MR-Brake-Based Haptic Device. *Smart Materials and Structures*, **15**, 1960-1966. https://doi.org/10.1088/0964-1726/15/6/052

[6] Karakoc, K., Park, E.J. and Suleman, A. (2008) Design Considerations for an Automotive Magnetorheological Brake. *Mechatronics*, **18**, 434-447. https://doi.org/10.1016/j.mechatronics.2008.02.003

[7] Park, E.J., Stoikov, D., Falcao da Luz, L. and Suleman, A. (2006) A Performance Evaluation of an Automotive Magnetorheological Brake Design with a Sliding Mode Controller. *Mechatronics*, **16**, 405-416. https://doi.org/10.1016/j.mechatronics.2006.03.004

[8] Park, E.J., da Luz, L.F. and Suleman, A. (2008) Multidisciplinary design optimization of an automotive magnetorheological brake design. *Computers & Structures*, **86**, 207-216. https://doi.org/10.1016/j.compstruc.2007.01.035

[9] Carlson, J.D. (2001) Magnetorheological Brake with Integrated Flywheel. US Patent No.6186290 B1. United States Patent Office.

[10] Nguyen, Q.H., Nguyen, N.D. and Choi, S. (2014) Optimal Design of a Novel Configuration of MR Brake with Coils Placed on the Side Housings. *SPIE Proceedings*. https://doi.org/10.1117/12.2044561

[11] Qin, H., Song, A. and Mo, Y. (2019) Evaluation of a Multi-Drum Magnetorheological Brake via Finite Element Analysis Considering Number of Drums and Fluid Gap Selection in Optimization. *Journal of Intelligent Material Systems and Structures*, **30**, 778-787. https://doi.org/10.1177/1045389x19828517

[12] Ngọc, N.A. (2016) Development and Analysis of New Multipole Magnetorheological Brake. Master's Thesis.

[13] Assadsangabi, B., *et al.* (2011) Optimization and Design of Disk-Type MR Brakes. *International Journal of Automotive Technology*, **12**, 921-932.

[14] Usoro, P.B., Smith, A.I., Moser, G. and Sommer, G. (2001) Magnetorheological Fluid Clutch. Patent US Patent Specification 6,318,531 B1.

[15] Güth, D., Schamoni, M. and Maas, J. (2013) Magnetic Fluid Control for Viscous Loss Reduction of High-Speed MRF Brakes and Clutches with Well-Defined Fail-Safe Behavior. *Smart Materials and Structures*, **22**, Article ID: 094010. https://doi.org/10.1088/0964-1726/22/9/094010

[16] Shamieh, H. and Sedaghati, R. (2018) Development, Optimization, and Control of a Novel Magnetorheological Brake with No Zero-Field Viscous Torque for Automotive Applications. *Journal of Intelligent Material Systems and Structures*, **29**, 3199-3213. https://doi.org/10.1177/1045389x18758186

[17] Park, E.J., da Luz, L.F. and Suleman, A. (2008) Multidisciplinary Design Optimization of an Automotive Magnetorheological Brake Design. *Computers & Structures*, **86**, 207-216. https://doi.org/10.1016/j.compstruc.2007.01.035

[18] Le-Duc, T., Ho-Huu, V. and Nguyen-Quoc, H. (2018) Multi-objective Optimal Design of Magnetorheological Brakes for Motorcycling Application Considering Thermal Effect in Working Process. *Smart Materials and Structures*, **27**, Article ID: 075060. https://doi.org/10.1088/1361-665x/aacb40

[19] Daoming, W., Lan, Y., Wenbin, S., Bin, Z. and Wuwei, C. (2019) Simulation and Experimental Study on Temperature Characteristics of Magnetorheological Fluid Brake for Vehicles. *Journal of Mechanical Engineering*, **55**, Article 100. https://doi.org/10.3901/jme.2019.06.100

[20] Patil, S.R., Powar, K.P. and Sawant, S.M. (2016) Thermal Analysis of Magnetorheological Brake for Automotive Application. *Applied Thermal Engineering*, **98**, 238-245. https://doi.org/10.1016/j.applthermaleng.2015.11.128

[21] Tuan, H.Q., Hoang, T.M. and Khoa, N.X. (2023) A Study the Effect of Key Parameters on the Magneto-Rheological Brake Torque Based on the Sim Method. *ARPN Journal of Engineering and Applied Sciences*, **18**, 1534-1538. https://doi.org/10.59018/0723192

[22] Lord Technical Data 2019 MRF-140CG Magneto-Rheological Fluid. https://www.lord.com

[23] Le-Duc, T. and Hung, N.Q. (2019) Design, Manufacturing and Testing of Magnetorheological Brake for Small Size Motorcycle. *The First International Conference on Material, Machines and Methods for Sustainable Development*, Danang, 18-19 May 2018. https://www.researchgate.net/publication/330292202

[24] Shiao, Y. and Nguyen, Q. (2013) Development of a Multi-Pole Magnetorheological Brake. *Smart Materials and Structures*, **22**, Article ID: 065008. https://doi.org/10.1088/0964-1726/22/6/065008